

# Scattering from objects immersed in a diffusive medium.

David Lancaster<sup>(a)</sup> and Theo Nieuwenhuizen<sup>(b)</sup>

Van der Waals–Zeeman Instituut,  
University of Amsterdam,  
Valkenierstraat 65,  
1018XE Amsterdam.

**Abstract:** The disturbance of the transmission of light through a diffusive medium due to an object hidden in it can be expressed in terms of an effective charge and dipole moment. In the mesoscopic regime, beyond the diffusion approximation, we calculate this effective charge and dipole moment. Various objects are considered: a single point scatterer, a localised density of such scatterers and a small sphere.

---

<sup>(a)</sup> (djl@ecs.soton.ac.uk)

<sup>(b)</sup> (niewenh@phys.uva.nl)

## 1. Introduction

The reconstruction of the properties of an object from data obtained in a scattering experiment is a problem that arises in all branches of physics. Here we consider the scattering of light from an object placed inside a diffuse medium. This poses problems because of the many further scattering events between object and observer; in everyday language, “the object cannot be seen”. However, with the help of sufficiently intense light sources, and careful and sensitive experimental techniques the small perturbations on the diffuse light due to the embedded object become detectable. For example experiments have been performed by den Outer, Nieuwenhuizen and Lagendijk [1]. The technological applications to non-invasive methods of detecting tumors in human flesh are active areas of research.

The significant feature of this work is that we go beyond the diffusion approximation discussed in [1] and make analytic calculations based on mesoscopic theory. This means that although the scattering length is much longer than the wavelength of the light ( $kl \gg 1$ ), we do not require that the relative size of the objects be much larger than the scattering length. Furthermore, we are able to impose boundary conditions based on the microscopic theory, which cannot be done in the diffusion approximation. We start with the simplest case, namely a point object. Our main result is for a small spherical object and we expect this result to be useful in providing an independent check of the numerical and other approximate approaches sometimes used in this field [2].

We make several simplifying assumptions: most importantly we only consider scalar waves and always assume isotropic scattering. Our results are presented in the form of the effective charge and dipole moment of the multipole expansion of the solutions of the diffusion equation in the far field region. This allows the results to be adapted to whatever detection arrangement is desired.

The paper starts with a description of the salient points of the mesoscopic multiple scattering formalism forming the basis of our analysis. The following sections, 3,4,5 consider a series of progressively more realistic objects: a point scatterer, a collection of such scatterers and a small sphere subject to a variety of boundary conditions. A short conclusion summarises our results.

## 2. Mesoscopic Scattering Formalism

We base our approach on the Schwarzschild Milne (SM) equation of radiation transfer theory. This equation may be obtained by integrating the full radiation transfer equation [3] but here we prefer to regard it as a Bethe Salpeter-like integral equation for the diffuse intensity  $J(\mathbf{r})$ . We write it in the general form,

$$J(\mathbf{r}) = S(\mathbf{r}) + \int d^3r' \mathcal{M}(\mathbf{r}, \mathbf{r}') J(\mathbf{r}'). \quad (2.1)$$

Where the source  $S$  and the kernel  $\mathcal{M}$  take different forms depending on the geometry of the problem. In the ladder approximation the kernel is given by the square of the amplitude green functions:  $\mathcal{M} = \frac{4\pi}{l} |G(\mathbf{r}, \mathbf{r}')|^2$ . A uniform density of scatterers leads to an amplitude green function  $G_0(r) = e^{i(k+i/2l)r}/4\pi r$ , where the scattering length  $l$  is related to the  $t$ -matrices of the individual scatterers and their density ( $n$ ) by  $l = 4\pi/nt\bar{t}$ . It is then simple to see that  $\mathcal{M}_0 = e^{-r/l}/4\pi l r^2$  (the SM equation is often stated for a slab geometry, and the relevant kernel is then obtained from  $\mathcal{M}_0$  by integrating over perpendicular momenta). The Fourier transform of this kernel is  $\tilde{\mathcal{M}}_0(q) = \tan^{-1}(ql)/ql$  ( $= A_1(ql)$  in the notation described in appendix C), so the green function  $\mathcal{G}_0$  for intensity propagation in the SM equation is  $\mathcal{G}_0(q) = 1/(1 - A_1(ql))$ . A fuller discussion of notation is provided in appendices A and B, and a general review of the formalism is given in [4].

In order to find the effect of an object embedded in the multiple scattering medium we require an expression for the appropriate SM kernel, which we base on a perturbative expansion of the amplitude green function. Firstly however, we consider exactly what quantity should be calculated to compare with measurements.

### 2.1. Measurement

We assume that system boundaries are distant from the localised region of the object. In this far field region, the diffuse intensity  $J(\mathbf{r})$  obeys the diffusion equation which is much simpler than the full SM equation. Since we are dealing with static quantities, the diffusion equation reduces to the Poisson equation.

$$\nabla^2 J(\mathbf{r}) = 0, \quad (2.2)$$

In the absence of the object, the solution of equation (2.2), subject to appropriate boundary conditions, is  $J_0(\mathbf{r})$ . The total intensity in the presence of the object then reads

$$J(\mathbf{r}) = J_0(\mathbf{r}) + \delta J(\mathbf{r}). \quad (2.3)$$

The goal of the present work is to characterise the disturbance  $\delta J(\mathbf{r})$  of the diffuse intensity, representing the diffuse image of the immersed object. We make use of the fact that the Poisson equation (2.2), allows electrostatic analogies, and represent the disturbance  $\delta J(\mathbf{r})$  in terms of a multipole series. It turns out that only the first two of them, namely the *charge*  $q$  and the *dipole*  $\mathbf{p}$ , play a role, while higher-order multipoles are negligible. Assume for a while that the turbid medium is infinite. The disturbance of the intensity far enough from an object placed at  $\mathbf{r}_0$  assumes the form

$$\delta J(\mathbf{r}) = \frac{q}{|\mathbf{r} - \mathbf{r}_0|} - \frac{\mathbf{p} \cdot (\mathbf{r} - \mathbf{r}_0)}{|\mathbf{r} - \mathbf{r}_0|^3}. \quad (2.4)$$

This expression, which is a solution of the diffusion equation (2.2), is also a solution of the full SM equation provided the distance from the object is large with respect to the mean free path  $l$ .

For a symmetric object, the linearity and isotropy of the problem imply that the charge and dipole have the form

$$q = -QJ_0(\mathbf{r}_0), \quad \mathbf{p} = -P\nabla J_0(\mathbf{r}_0). \quad (2.5)$$

We follow the notation proposed by J.M. Luck, and call  $Q$  the *capacitance* of the object, and  $P$  the *polarizability* [5]. These two numbers are intrinsic to the embedded object.

The capacitance  $Q$  is non-zero (and in fact positive) only if the sphere absorbs light. For a non-absorbing object, the leading contribution is that of the induced dipole  $\mathbf{p}$ . The corresponding polarizability  $P$  can be either positive or negative, depending on the nature of the object. Notice that  $Q$  has the dimension of a length, while  $P$  has the dimension of a volume.

For real measurements we should bear in mind that the diffusion approximation will break down in the vicinity of the measurement apparatus. For the particular case of a thick slab geometry, which is often encountered experimentally [1], we now recall the derivation of the diffuse image of a small object to show how the capacitance and polarizability can be measured,

The sample is a thick slab ( $0 < x < L$ ), with  $L \gg l$ , assumed to be infinite in the two transverse directions. We set  $\rho = (y^2 + z^2)^{1/2}$ . The left side of the sample ( $x = 0$ ) is subject to an incident plane wave, so that the solution of eq. (2.2) when the immersed object is absent reads

$$J_0(\mathbf{r}) = J \left( 1 - \frac{x}{L} \right). \quad (2.6)$$

The intensity  $T(y, z)$  transmitted through the sample, and emitted on the right side ( $x = L$ ) at the point  $(y, z)$ , is proportional to the derivative  $\partial J(x = L, y, z)/\partial x$ . When there is no immersed object, eq. (2.6) yields a uniform transmission  $T_0 = Kl/L$ . The prefactor  $K$  describes the angular dependence of the transmitted intensity. It also depends on microscopic characteristics of the medium, such as any anisotropy of the scatterers.

Let the immersed object have capacitance  $Q$  and polarizability  $P$ , and be located at  $x = x_0, y = z = 0$ . Its charge and dipole then read

$$q = -QJ \left(1 - \frac{x_0}{L}\right), \quad \mathbf{p} = \frac{PJ}{L} \hat{x}, \quad (2.7)$$

with  $\hat{x}$  being the unit vector of the positive  $x$ -axis.

Along the lines of ref. [1], the total intensity can be determined by summing the free-space expression (2.4) over an infinite double array of images ( $-\infty < n < +\infty$ ). We thus obtain

$$J(\mathbf{x}) = J \left(1 - \frac{x}{L}\right) + q \sum_n \left( \frac{1}{[(x - x_0 + 2nL)^2 + \rho^2]^{1/2}} - \frac{1}{[(x + x_0 + 2nL)^2 + \rho^2]^{1/2}} \right) - \frac{PJ}{L} \sum_n \left( \frac{x - x_0 + 2nL}{[(x - x_0 + 2nL)^2 + \rho^2]^{3/2}} + \frac{x + x_0 + 2nL}{[(x + x_0 + 2nL)^2 + \rho^2]^{3/2}} \right). \quad (2.8)$$

The transmitted intensity  $T(y, z) = T(\rho)$  then reads

$$T(\rho) = T_0 \left( 1 - 2Q(L - x_0) \sum_n \frac{L - x_0 + 2nL}{[(L - x_0 + 2nL)^2 + \rho^2]^{3/2}} - 2P \sum_n \frac{2(L - x_0 + 2nL)^2 - \rho^2}{[(L - x_0 + 2nL)^2 + \rho^2]^{5/2}} \right). \quad (2.9)$$

Such characteristic profiles have been observed experimentally for the case of pencils (black cylinders) and glass fibers (transparent cylinders with index mismatch) by den Outer et al.

In order to calculate the charge and dipole moment in terms of microscopic properties of the object we relate (2.4) to the far field behaviour of the full SM equation with the same incoming intensity. At first order, an object placed in the medium modifies the free kernel

of the SM equation by adding a vertex term  $\mathcal{M} = \mathcal{M}_0 + V$ , which for small momenta we can write<sup>1</sup> as,

$$V(\mathbf{p}, \mathbf{p}') = \frac{4\pi l^2}{3} (-Q + P\mathbf{p}\cdot\mathbf{p}'). \quad (2.10)$$

The parameters  $Q$  and  $P$  are precisely the ones that appear in the multipole expansion (2.4). To see this, insert the expansion of the kernel,  $\mathcal{M} = \mathcal{M}_0 + V$ , into the the SM equation and solve perturbatively for the far field intensity  $J(\mathbf{r})$ . This can be done using the diffusion limit of the free intensity green function,  $\tilde{\mathcal{G}}_0(r) \propto 1/r$ . We emphasise the perturbative nature of this general result, and indeed it fails in the case of a large spherical object. This will be the reason for later restricting our attention to a small sphere.

In the rest of the paper we will define the vertex more precisely and develop a diagrammatic perturbation expansion of the SM equation to calculate it both at leading and higher order. Only the small momentum behavior of the vertex is important for our goal of calculating  $Q$  and  $P$ , and we shall find that in this case the higher order corrections can sometimes be resummed.

### 3. Additional Point-Like Scatterer

The effect of an object consisting of a single point-like scatterer is a worthwhile exercise because it allows us to demonstrate the method in a simple setting. Although the higher order terms can be formally calculated, they are not reliable since we encounter ill-defined expressions arising from the point-like limit which take us out of the realm of validity of the mesoscopic theory.

#### 3.1. Leading Order Calculation

Starting from the amplitude green function for a single extra scatterer with  $t$ -matrix  $t_e$ , at the origin,

$$G(\mathbf{r}, \mathbf{r}') = G_0(|\mathbf{r} - \mathbf{r}'|) + G_0(\mathbf{r})t_e G_0(\mathbf{r}'). \quad (3.1)$$

The full SM kernel is given by,

$$\mathcal{M}(\mathbf{r}, \mathbf{r}') = \mathcal{M}_0 + \delta\mathcal{M} = \frac{4\pi}{l}|G|^2 = \frac{4\pi}{l}|G_0(|\mathbf{r} - \mathbf{r}'|) + G_0(\mathbf{r})t_e G_0(\mathbf{r}')|^2. \quad (3.2)$$

---

<sup>1</sup> We define the Fourier transform so that the first momentum is incoming and the second outgoing.

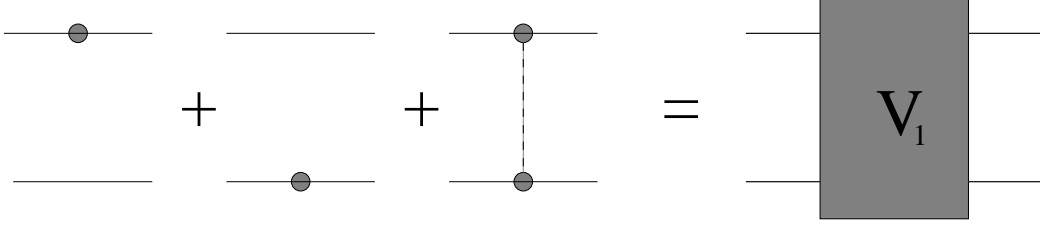


**Fig. 1:** Diagrams contributing to the bare vertex  $V_1$ .

The diagrammatic interpretation is obvious and the vertex (2.10) contains the terms shown in figure 1. All terms will be the same order due to the optical theorem. If we evaluate the diagrams in momentum space we may use the formulae in appendix B to obtain the mesoscopic limit,

$$V_1(\mathbf{p}, \mathbf{p}') = \delta\tilde{\mathcal{M}}(\mathbf{p}, \mathbf{p}') = l \left( \frac{t_e \bar{t}_e}{4\pi} A_1(pl) A_1(p'l) + \frac{i(t_e - \bar{t}_e)}{2k} A_2(\mathbf{pl}, \mathbf{p}'l) \right). \quad (3.3)$$

Now we use the optical theorem as applied to the additional scatterer. We allow this extra scatterer to have a complex refractive index and introduce the albedo  $a_e$  which appears in the optical theorem:

$$\sigma_{el} = \frac{t_e \bar{t}_e}{4\pi} = a_e \frac{\Im m t_e}{k} \quad (3.4)$$

Where  $\sigma_{el}$  is the elastic contribution to the cross section for the additional scatterer.

The final expression for the bare vertex is,

$$V_1(\mathbf{p}, \mathbf{p}') = l \sigma_{el} \left( A_1(pl) A_1(p'l) - \frac{1}{a_e} A_2(\mathbf{pl}, \mathbf{p}'l) \right) \quad (3.5)$$

By using the small momentum expansions of the  $A_i$  functions given in appendix C, we are able to identify the charge and dipole moment defined by equation (2.10),

$$\begin{aligned} Q_1 &= \frac{\sigma_{el}}{l} \frac{3}{4\pi} (1/a_e - 1) = \frac{3}{4\pi} \frac{\sigma_{abs}}{l} \\ P_1 &= \sigma_{el} l \frac{1}{4\pi} (1/a_e) = \frac{1}{4\pi} \sigma_{tot} l \end{aligned} \quad (3.6)$$

For albedo  $a_e < 1$ , there is absorption and the charge is positive.

### 3.2. Second Order Correction

This expression for the vertex,  $V_1 = \delta\mathcal{M}$ , is only the first term in the perturbative expansion of the SM equation. Higher order terms contain these vertices connected by intensity propagators in the form  $V_n = V_1\mathcal{G}_0V_1\dots V_1\mathcal{G}_0V_1$ . In general these vertices are not easy to evaluate because the intermediate loop integrals do not give rise to closed expressions. However, for the multipole expansion we only require the behaviour for small external momentum and can therefore approximate the first and last  $V_1(\mathbf{p}, \mathbf{p}')$ . In this case, the angular integration over the intermediate momenta simplifies the expressions remarkably so that the effect propagates through the series making it valid for each loop as shown below.

For small incoming momentum,  $p$ , we can expand the bare vertex using the expansion of  $A_2$  in appendix C. This leaves  $V_1(\mathbf{p}, \mathbf{p}')$  written in terms of  $A_1(p')$  and explicit factors of momenta:  $p^2$ ,  $p'^2$  and  $\mathbf{p}\cdot\mathbf{p}'$ . Let us work to first order in  $p$  in which case,

$$V_1(\mathbf{p}, \mathbf{p}') \xrightarrow{p \rightarrow 0} -\frac{4\pi l^2}{3}Q_1A_1(p'l) + \mathbf{p}\cdot\mathbf{p}'4\pi l^2P_1A_3(p'l) \quad (3.7)$$

where  $Q_1$  and  $P_1$  are given above in (3.6) and we have employed the useful combination  $A_3(q) = (1 - A_1(q))/q^2$ .

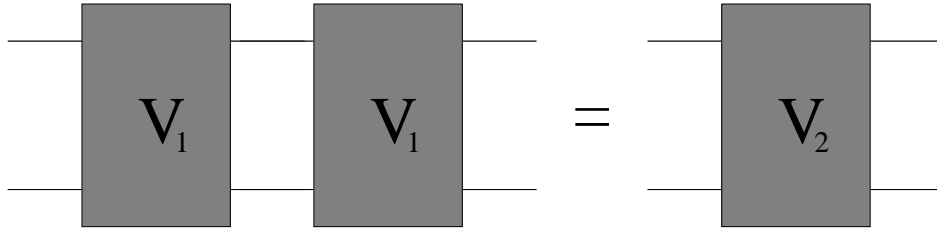


**Fig. 2:** The second order vertex  $V_2$ , is composed of two first order vertices.

Now consider the second order contribution shown in figure 2,

$$V_2(\mathbf{p}, \mathbf{p}') = \int \frac{d^3q}{(2\pi)^3} V_1(\mathbf{p}, \mathbf{q})\mathcal{G}_0(q)V_1(\mathbf{q}, \mathbf{p}') \quad (3.8)$$

where  $\mathcal{G}_0$  is the free propagator as discussed in section 2. Using the approximate expression (3.7) in the first factor of  $V_1$  the integrals become tractable. Performing the angular part of the integral using the formulae given in appendix C we find that the general form of  $V$  is preserved,

$$V_2(\mathbf{p}, \mathbf{p}') = -\frac{4\pi l^2}{3}Q_2A_1(p'l) + \mathbf{p}\cdot\mathbf{p}'4\pi l^2P_2A_3(p'l) \quad (3.9)$$



where the explicit expressions for  $Q_2$  and  $P_2$  are,

$$\begin{aligned} Q_2 &= \frac{\sigma_{el}}{l} \left( \frac{1}{a_e} - 1 \right) B_1 Q_1 = -\frac{4\pi}{3} B_1 Q_1^2 \\ P_2 &= -\sigma_{el} \left( \frac{1}{a_e l^2} \right) B_2 P_1 = -4\pi B_2 P_1^2 \end{aligned} \quad (3.10)$$

The remaining integrations over the magnitude of the momenta are contained in the dimensionless factors  $B_1$  and  $B_2$ , where in the second expressions we have used the explicit form of  $\mathcal{G}_0(q)$ .

$$\begin{aligned} B_1 &= \frac{l^2}{2\pi^2} \int dq q^2 A_1^2(q) \mathcal{G}_0(q) = \frac{1}{2\pi^2 l} \int_0^{\Lambda} dq q^2 \frac{A_1^2(q)}{(1 - A_1(q))} \\ B_2 &= \frac{1}{2\pi^2} \int dq q^2 A_3^2(q) \mathcal{G}_0(q) = \frac{1}{2\pi^2 l^3} \int_0^{\Lambda} dq (1 - A_1(q)) \end{aligned} \quad (3.11)$$

Here we encounter a problem due to the point-like limit. The integrals diverge linearly, so we have introduced a high momentum regulator  $\Lambda$  which we expect to be of the order of the inverse size of the scatterer,  $\Lambda \sim 1/R$ . For the point-like analysis above to be valid, the size of the extra scatterer must be much less than the wavelength,  $R \ll \lambda$ . This means that very high momenta, up to the inverse scale of the scatterer, are encountered in the integral and in this range the mesoscopic approximation fails. The expressions for the second order terms are therefore formal. A similar divergence arises for the  $t$ -matrix of a point scatterer [6], where it was parametrised as a linear divergence depending on some property of the scatterer. The problem of divergencies will not appear in the following sections where we will consider extended objects.

### 3.3. Higher Order Corrections

Bearing in mind the caveats above, we proceed formally to illustrate how the higher order effects may be calculated. Since the form of the vertex remains the same as additional bubbles are added, it is clear that the full series can be summed to obtain an expression for the full  $V$ . The explicit expressions for  $Q$  and  $P$  are then,

$$\begin{aligned} Q &= \frac{Q_1}{1 + \frac{\sigma_{el}}{l}(1/a_e - 1)B_1} = \frac{Q_1}{1 + \frac{4\pi}{3}Q_1 B_1} \\ P &= \frac{P_1}{1 + 3\sigma_{el}l(1/a_e)B_2} = \frac{P_1}{1 + 4\pi P_1 B_2} \end{aligned} \quad (3.12)$$

It is interesting to note that if the capacitance  $Q$  is negative (corresponding to amplification rather than absorption) it could be substantially enhanced by these higher order effects.

### 3.4. Maximally Crossed Diagrams

Because we are dealing with the peculiar situation of a point-like object another issue becomes important, which although academic is interesting to discuss. Crossed diagrams generally play a sub-leading role in mesoscopic calculations, for example in the ladder propagator it can be seen that crossed diagrams contribute at higher order in  $1/kl$ . This conclusion must be reexamined for the point object and diagrams in real space show that the crossed diagrams can contribute at the same order as uncrossed ones. This can be understood as being due to the phase cancelling in the same way as it does for enhanced backscattering. These contributions only occur when maximally crossed series are inserted between two additional scatterers on the same line (there can be an extra scatterer on the other line or not). In this case, each diagram contributes exactly as for the ladder sum. The previous calculation must be generalised so that crossed diagrams are not included between additional scatterers on different lines. This combinatoric problem may be solved using a matrix formalism described in Appendix D and the final result in the mesoscopic limit is that the charge and dipole in that case are as above but  $B$  gains a factor of 2.

These calculations illustrate how the full sum can be calculated from an infinite series of diagrams. Unfortunately the results are flawed because the divergences due to the point nature of the object take the calculation out of the realm of validity of the mesoscopic approximation. In the next sections we will consider better defined systems.

## 4. Many Extra Scatterers

We now consider an object consisting of a collection of extra point-like scatterers localised in some region of size  $R$ . We first develop perturbation theory for the amplitude green functions which we then use in the kernel of the SM equation.

### 4.1. Perturbative expansion

Consider extra scatterers placed in a localised region with density profile  $n_e(\mathbf{r})$ . The perturbative expansion of the amplitude green function in terms of the individual extra scatterer t-matrix  $t_e$ , resembles the expression (3.1),

$$G(\mathbf{r}, \mathbf{r}') = G_0(|\mathbf{r} - \mathbf{r}'|) + t_e \int d^3r'' G_0(|\mathbf{r} + \mathbf{r}''|) n_e(r'') G_0(|\mathbf{r}'' - \mathbf{r}'|) + \dots \quad (4.1)$$

Where, as usual,  $G_0$  is the green function in the presence of a constant density of background scatterers. In momentum space we have,

$$\begin{aligned}\tilde{G}(\mathbf{p}, \mathbf{p}') &= \delta(\mathbf{p} - \mathbf{p}')G_0(\mathbf{p}) + \tilde{n}_e(\mathbf{p} - \mathbf{p}')t_e G_0(\mathbf{p})G_0(\mathbf{p}') \\ &+ \int \frac{d^3q}{(2\pi)^3} \tilde{n}_e(\mathbf{p} - \mathbf{q})\tilde{n}_e(\mathbf{q} - \mathbf{p}')t_e^2 G_0(\mathbf{p})G_0(\mathbf{q})G_0(\mathbf{p}') + \dots\end{aligned}\quad (4.2)$$

We use the above expression to find a form for the SM kernel. Here we must be careful to include an extra term in the definition of the kernel because the amplitude lines may end on an extra rather than background scatterer; to the factor  $4\pi/l$  interpreted as  $n|t_e|^2$ , we must add the contribution of the extra scatterers  $n_e(r)|t_e|^2$ .

$$\begin{aligned}\mathcal{M}(\mathbf{r}, \mathbf{r}') &= \left( \frac{4\pi}{l} + n_e(r)|t_e|^2 \right) |G(\mathbf{r}, \mathbf{r}')|^2 \\ \tilde{\mathcal{M}}(\mathbf{p}, \mathbf{p}') &= \frac{4\pi}{l} \int \frac{d^3q}{(2\pi)^3} \frac{d^3q'}{(2\pi)^3} \bar{G}(\mathbf{q} + \mathbf{p}, \mathbf{q}' + \mathbf{p}')G(\mathbf{q}, \mathbf{q}') \\ &+ |t_e|^2 \int \frac{d^3q}{(2\pi)^3} \frac{d^3q'}{(2\pi)^3} \frac{d^3q''}{(2\pi)^3} \tilde{n}_e(\mathbf{q}'')\bar{G}(\mathbf{q} + \mathbf{p}, \mathbf{q}' + \mathbf{q}'' + \mathbf{p}')G(\mathbf{q}, \mathbf{q}')\end{aligned}\quad (4.3)$$

In this problem, the vertex that relates the mesoscopic SM calculation to the multipole expansion (2.4) is not simply given by  $V = \delta\mathcal{M}$  as it was for the single point object. In the far-field region where the identification is made, there are no extra scatterers, so we must insist that the vertex only contain diagrams which end on a background rather than extra scatterer. This prescription is most easily viewed diagrammatically rather than in terms of the formal perturbation expansion of the SM equation and its effect is also to remove the asymmetry apparent in the kernel itself.

Another difference with the point scatterer case is that the perturbation expansion is organised in powers of the extra density factor  $n_e(r)$ , and we are unable to relate different orders with the Optical theorem. The additional term included in (4.3) saves the situation. Inserting the expansion of the green function and identifying the first order term  $\mathcal{M}_1$ , the additional term also contributes as the last term below.

$$\begin{aligned}\tilde{\mathcal{M}}_1(\mathbf{p}, \mathbf{p}') &= \frac{4\pi}{l} \int \frac{d^3q}{(2\pi)^3} \frac{d^3q'}{(2\pi)^3} \\ &t_e \tilde{n}_e(q - q')G_0(\mathbf{q})G_0(\mathbf{q}')\bar{G}_0(\mathbf{q} + \mathbf{p})\delta(\mathbf{q} + \mathbf{p} - \mathbf{q}' - \mathbf{p}') \quad + \text{c.c.} \\ &+ |t_e|^2 \tilde{n}_e(p - p') \int \frac{d^3q}{(2\pi)^3} G_0(\mathbf{q})\bar{G}_0(\mathbf{q} + \mathbf{p})\end{aligned}\quad (4.4)$$

This expression can be simplified using the functions  $A_i$  defined in appendix B and C. In order to obtain  $V_1$  from  $\mathcal{M}_1$ , we make a small modification to the second term in order that it end on a background scatterer.

$$\begin{aligned} V_1(\mathbf{p}, \mathbf{p}') &= \left( \frac{4\pi}{l} it_e \tilde{n}_e(\mathbf{p} - \mathbf{p}') \frac{l^2}{8\pi k} A_2(\mathbf{pl}, \mathbf{p'l}') + \text{c.c.} \right) + |t_e|^2 \tilde{n}_e(\mathbf{p} - \mathbf{p}') \frac{l}{4\pi} A_1(pl) A_1(p'l') \\ &= \tilde{n}_e(\mathbf{p} - \mathbf{p}') l \sigma_{el} \left( A_1(pl) A_1(p'l') - \frac{1}{a_e} A_2(\mathbf{pl}, \mathbf{p'l}') \right) \end{aligned} \quad (4.5)$$

The second line follows from the optical theorem applied to the individual scatterers, as in the point scatterer case. We can immediately identify the charge and dipole at this order by taking the momenta small and using the definition (2.10).

$$\begin{aligned} Q_1 &= \frac{\sigma_{el}}{l} \frac{3}{4\pi} N_e (1/a_e - 1) = N_e Q_1^{\text{point object}} \\ P_1 &= \sigma_{el} l \frac{1}{4\pi} N_e \left( 1/a_e - 6 \frac{R^2}{l^2} (1/a_e - 1) \right) = N_e P_1^{\text{point object}} - 2N_e R^2 Q_1^{\text{point object}} \end{aligned} \quad (4.6)$$

Where  $N_e = \tilde{n}_e(0)$  is the total number of extra scatterers. The second term in  $P_1$  comes from expanding the density form factor for small momentum as  $\tilde{n}_e(p) \approx N_e(1 - p^2 R^2)$ , and  $R$  is a measure of the size of the object,  $R^2 = \frac{4\pi}{3N_e} \int r^4 n_e(r) dr$ . A more precise expression can be obtained if we assume a particular density profile, for example a Gaussian form. We have assumed a spherically symmetric density perturbation so  $\tilde{n}_e(p)$  is real. The similarity with the single scatterer result (3.6) is clear; the charge merely gets multiplied by the number of scatterers present whereas the dipole moment also picks up a term that depends on the size of the object.

#### 4.2. Second Order

Two types of term occur at second order, those from second order in the expansion of the amplitude green function, and those from first order in the expansion of the amplitude green function but second order in the expansion of the SM equation.

The first type of term can be neglected because for example one contribution to the charge is,

$$\frac{4\pi}{l} |t_e|^2 \int \frac{d^3 q}{(2\pi)^3} \frac{d^3 q'}{(2\pi)^3} |\tilde{n}_e(\mathbf{q} - \mathbf{q}')|^2 |G_0(\mathbf{q})|^2 |G_0(\mathbf{q}')|^2 \quad (4.7)$$

which corresponds to processes in which the amplitudes scatter off different extra scatterers so the phase cancelation kills them. This can be seen explicitly for a Gaussian profile, where

the contribution will be of order  $\sigma_e/l^2 \times N_e^2/k^2R^2$ . By comparing with the main second order contributions below we obtain a condition on the size of object for this analysis to remain valid,  $k^2R^2(1 - 1/a_e)B_1Q_1^{point\ object} \gg 1$ .

We therefore only consider the term with the form  $V_2 = V_1\mathcal{G}V_1$ . Note that although this is clear diagrammatically, at the level of the formal expansion the correction we made to obtain  $V_1$  from  $\mathcal{M}_1$  appears in  $V_1\mathcal{G}V_1$  in just the right way to count the relevant terms in  $\mathcal{M}_2$ , which need not be evaluated separately. We attempt to use the same trick as for the point scatterer and therefore expand the bare vertex for small incoming momentum  $p$ ,

$$V_1(\mathbf{p}, \mathbf{p}') \xrightarrow{p \rightarrow 0} \tilde{n}_e(\mathbf{p} - \mathbf{p}') \left( -\frac{4\pi l^2}{3} Q_1^{point\ object} A_1(p'l) + \mathbf{p} \cdot \mathbf{p}' 4\pi l^2 P_1^{point\ object} A_3(p'l) \right) \quad (4.8)$$

Now consider the first diagram,

$$V_2(\mathbf{p}, \mathbf{p}') = \int \frac{d^3q}{(2\pi)^3} V_1(\mathbf{p}, \mathbf{q}) \mathcal{G}(q) V_1(\mathbf{q}, \mathbf{p}') \quad (4.9)$$

Because of the presence of the density form factor, the angular integrals that kept the form of  $V$  the same at higher order and therefore allowed us to perform the full sum in the point scatterer case cannot be done. Let us instead do the second order calculation by setting *both* the external momenta small. The final expressions for  $Q_2$  and  $P_2$  are then,

$$\begin{aligned} Q_2 &= \frac{\sigma_e}{l} N_e \left( 1 - \frac{1}{a_e} \right) B_1 Q_1 \\ P_2 &= \sigma_e l N_e \frac{1}{a_e} B_2 P_1 - 2R^2 Q_1 \end{aligned} \quad (4.10)$$

Where the factors  $B$  are now well-defined and do not need regulating because the density acts as a smooth cutoff at momenta of order  $1/R$ . In this regime the mesoscopic approximation is still valid so the approach is consistent.

$$\begin{aligned} B_1 &= \frac{1}{2\pi^2 N_e^2 l} \int_0^\infty dq q^2 \tilde{n}_e^2(q/l) \frac{A_1^2(q)}{(1 - A_1(q))} \\ B_2 &= \frac{1}{2\pi^2 N_e^2 l^3} \int_0^\infty dq \tilde{n}_e^2(q/l) (1 - A_1(q)) \end{aligned} \quad (4.11)$$

This resolves the difficulties encountered in the point object case, but the discussion above shows that we cannot write simple expressions for terms higher than second order. Crossed diagrams are also suppressed in this case.

## 5. Spherical Object

We consider the simplest example of an extended object immersed in the multiple scattering background: a sphere of radius  $R$  ( $kR \gg 1$ ) subject to a variety of boundary conditions. The analogous problem in a free background was much studied in the early part of this century [7], and some of the results relevant to the present problem are collected in appendix E.

The general result relating the effective charge to the fourier transformed vertex is perturbative about the free theory, but depending on the boundary conditions, the interior region of a finite size object may not be susceptible to such treatment. For example, for reflecting boundary conditions the full green function in the interior vanishes, which cannot be regarded as a small correction. A different approximation scheme, or an object with similar refractive index to the medium could be considered, but here we shall proceed by assuming that the sphere is small:  $R \ll l$ . In this case it can be argued that the correction from the interior of the sphere is smaller than the perturbative term we shall calculate. This limit is the opposite of the limit in which diffusion theory is valid. An alternative approach to this problem is to use radiative transfer theory and boundary conditions for the intensity field [5].

### 5.1. Leading Order

Employing spherical polar coordinates we write the amplitude Green function in terms of spherical harmonics and spherical Bessel functions,

$$G(\mathbf{r}, \mathbf{r}') = \sum_{lm} g_l(r, r') Y_{lm}(\theta, \phi) \bar{Y}_{lm}(\theta', \phi') \quad (5.1)$$

$$g_l(r, r') = g_l^{(0)}(r, r') + a_l g_l^{(1)}(r, r') = ik(j_l(kr_{<}) + a_l h_l^{(1)}(kr_{<})) h_l^{(1)}(kr_{>})$$

Where the notation  $r_{>}, r_{<}$  indicates the larger or smaller of the two radii  $r, r'$ . As usual,  $k$  has an imaginary part to take account of multiple scattering, but on the surface of the sphere where the boundary conditions determining the coefficients  $a_l$  are imposed, the value of  $k$  must be reconsidered. In a fully self consistent approach, the imaginary part of  $k$  is fixed by the return green function  $G(\mathbf{r}, \mathbf{r})$  [4], and can vary in space. This variation is only significant close to the surface of the extended object and in the mesoscopic approximation it can be ignored<sup>2</sup>, thus justifying the form (5.1). At the surface however,

---

<sup>2</sup> In a one-dimensional version of the problem this can be an important effect.

where the boundary conditions are imposed, the self consistent form of  $k$  must be used. For example Dirichlet ( $D$ ) and Neumann ( $N$ ) conditions which correspond to reflections, have  $k$  real at the boundary and lead to  $a_l^{D,N} = -(1 \mp (-1)^l e^{-2ikR})/2$ . More general boundary conditions, mimicking the matching of internal and external solutions, can be imposed by introducing a surface impedance.

In the same way as for the point-like object of section 3, the bare vertex of the SM equation is given by,

$$V_1(\mathbf{r}, \mathbf{r}') = \frac{4\pi}{l} \left( |G(\mathbf{r}, \mathbf{r}')|^2 - |G^{(0)}(\mathbf{r}, \mathbf{r}')|^2 \right) \quad (5.2)$$

Where  $G^{(0)}$  is the free green function, given by the same expansion as (5.1) with  $a_l = 0$ . According to (2.10), the charge  $Q$  is related to the Fourier transform of this vertex at vanishing momenta. This perturbative result is clearly inappropriate in the interior of the sphere where  $G(\mathbf{r}, \mathbf{r}')$  vanishes, nonetheless corrections from the interior should not exceed  $O(R/l)^3$ , and can be neglected in comparison with the leading term for small spheres. Using orthogonality properties of the spherical harmonics, the charge can be written as a sum of radial integrals over products of  $g_l^{(0)}(r, r')$  and  $g_l^{(1)}(r, r')$ . These integrals may be simplified using the asymptotic form of the Bessel functions valid since  $kR \gg 1$ . This asymptotic approximation is only good for angular momentum numbers  $l < l_{max}$ , where  $l_{max} = kR$ , which in any case forms a effective upper limit in the angular momentum sum since the  $a_l$ 's become small for higher  $l$  (this approximation is standard in dealing with scattering from spheres). Dropping subleading terms in  $1/kl$  we find,

$$Q_1 = \frac{-3}{4\pi l^2} \int_R \int_R dr^3 dr'^3 V_1(\mathbf{r}, \mathbf{r}') = \frac{e^{-2R/l}}{(kl)^2} \sum_l^{l_{max}} (2l+1) \left( \frac{a_l + \bar{a}_l}{2} + |a_l|^2 \right) \quad (5.3)$$

The combination of  $a_l$ 's is recognisable from the classical amplitude scattering problem where a similar sum appears in the absorption cross section. Using this result, and only keeping the leading term in  $R/l$ , we find,

$$Q_1 = \frac{3}{4\pi} \frac{\sigma_{abs}}{l} \quad (5.4)$$

Where  $\sigma_{abs}$  is the absorption cross section. It is reassuring that this coincides with the point-like result (3.6). In particular, for a black (totally absorbing) sphere one has  $\sigma_{abs} = \pi R^2$ . This implies  $Q_1 = 3R^2/4l$ , a result derived already in [8].

For the  $D$  and  $N$  boundary conditions the charge must vanish since they correspond to reflection. There is no absorption and indeed each term in the sum (5.3) vanishes when the explicit forms of  $a_l^{D,N}$  are used. The calculation of  $\sigma_{abs}$  in the case of more general boundary conditions (for example a surface impedance) is a standard problem, the only subtlety arising from the value of  $k$  at the boundary.

The dipole moment can be calculated in a similar way. We find the general result,

$$P_1 = \frac{1}{4\pi l^2} \frac{\partial}{\partial p} \cdot \frac{\partial}{\partial p'} \tilde{V}_1|_0 = -(R+l)^2 \frac{e^{-2R/l}}{k^2 l} \sum_l^{l_{max}} \left( (2l+1) \frac{a_l + \bar{a}_l}{2} + (l+1)(a_l \bar{a}_{l+1} + \text{c.c.}) \right) \quad (5.5)$$

The first term in the sum is recognised as the total cross section  $\sigma_{tot} = 2\pi R^2$ , but the second term is a combination that never appears in the amplitude problem. For boundary conditions based on a surface impedance we can show that this second term is proportional to the absorption cross section (and therefore vanishes for  $D$  or  $N$  boundary conditions). Taking only the leading order terms we may write the dipole as,

$$P_1 = \frac{\sigma_{tot} l}{4\pi} - \frac{Q_1 l^2}{3} \quad (5.6)$$

The first term recovers the point object result in the limit  $R \ll l$ , whereas the second term is reminiscent of the similar term in the formula (4.6) for a collection of point scatterers. In case of a small reflecting but non-absorbing sphere we have  $\sigma_{tot} = 2\pi R^2$ , and we find  $P_1 = R^2 l/2$ .

## 5.2. Higher order

We may sum all the higher order corrections to the charge and dipole moment following the same method as for the point scatterer. In this case we do not have an explicit form for the Fourier transform of the vertex so intermediate formulae are unwieldy. We start with the form of the vertex for small incoming momentum in analogy to formula (3.7).

$$V_1(\mathbf{p}, \mathbf{p}') \xrightarrow{p \rightarrow 0} -\frac{4\pi l^2}{3} Q_1 A_1^{(R)}(p'l, R/l) + \mathbf{p} \cdot \mathbf{p}' 4\pi l^2 P_1 A_3^{(R)}(p'l, R/l) \quad (5.7)$$

Where we have introduced functions  $A_1^{(R)}(p'l, R/l)$  and  $A_3^{(R)}(p'l, R/l)$ , defined in appendix F. These functions become the point scatterer functions  $A_1, A_3$  in the limits of small  $R$ , but are better behaved at large momenta thus avoiding the problems encountered with the point object.



A calculation of the second order vertex at small incoming momentum shows that it retains the same form as (5.7). This calculation requires various integrals that are collected in appendix F. Proceeding by iteration the full sum can be performed exactly in the same way as for the point object. Our final result takes the same form as (3.12):

$$\begin{aligned} Q &= \frac{Q_1}{1 + \frac{4\pi}{3} Q_1 B_1} \\ P &= \frac{P_1}{1 + 4\pi P_1 B_2} \end{aligned} \tag{5.8}$$

Where the integrals over the magnitude of the momentum are now given in terms of the modified functions  $A^R$ .

$$\begin{aligned} B_1 &= \frac{l^2}{2\pi^2} \int_0^\infty dq q^2 \mathcal{G}_0(q) (A_1^{(R)}(ql, R/l))^2 \\ B_2 &= \frac{l^2}{2\pi^2} \int_0^\infty dq q^4 \mathcal{G}_0(q) (A_3^{(R)}(ql, R/l))^2 \end{aligned} \tag{5.9}$$

These integrals are well behaved for finite  $R/l$  and the major contribution comes from the region in which the mesoscopic calculation is valid. This therefore resolves the difficulty encountered with the point scatterer, but the result is only valid for small  $R/l$ .

## 6. Conclusion

In the mesoscopic regime, we have shown how to calculate the effective charge and dipole moment that would be seen in the change of the transmitted light due to some simple objects placed inside a diffuse medium. The simplest calculation was for a single point scattering object. In this case we were able to sum up all higher order terms in the perturbative expansion (in the strength of the vertex) which contributed to leading order in the mesoscopic approximation. However, the point nature of the scatterer was incompatible with the mesoscopic approximation and this was reflected in the divergent result. To resolve this problem we considered extended objects. A collection of point scatterers gave finite results, but it was not possible to analytically sum all the higher order terms. We therefore turned to a spherical object and our main results are the formulae (5.8) for the charge and dipole moment of a small sphere in a multiple scattering medium. These results include an infinite sum of higher order corrections and despite the many simplifying assumptions that went into their derivation, they should be useful as an independent check of the numerical methods in common use.

## **Acknowledgements**

This research originated from a pleasant discussion T.M. Nieuwenhuizen had with the late Shechao Feng. We would like to acknowledge useful discussions with J.M. Luck.

## Appendix A. Notation

In this appendix we recall some basic definitions. The background scatterers that compose the diffuse medium have a density  $n$  and are individually described by the t-matrix  $t$ . The mean free path  $l$  is related to the elastic cross section by  $l = 1/n\sigma_{el} = 4\pi/nt\bar{t}$ . The green function for amplitude propagation in this medium has its wavevector shifted away from the value  $k^2 = \omega^2\epsilon_0$  of the free scalar wave equation,  $\nabla^2\psi + k^2\psi = 0$ , to obtain  $G_0(\mathbf{p}) = (p^2 - k^2 - nt)^{-1} = (p^2 - k_R^2 - ik_R/l_{ex})^{-1}$ . In the second form we have explicitly split the t-matrix into its real and imaginary parts. The real part acts to shift the frequency,  $k_R^2 = k^2 + n\Re t$ . This effect is ordinarily described by an index of refraction, we shall take this as understood and drop the subscript on  $k$ . The small imaginary part of the t-matrix is most important and is related by the optical theorem to the total cross section including both the effect of elastic scattering and absorption, this is described by the extinction mean free path,  $n\Im t/k = 1/l_{ex}$ . Absorption is traditionally described by an albedo factor that relates the absorption and elastic cross section by  $\sigma_{el} = a\sigma_{tot}$  or  $\sigma_{abs} = (1/a - 1)\sigma_{el}$  and also the mean free paths,  $l_{ex} = al$ . We shall only allow absorption by the extra, not background, scatterers. The optical theorem and relation to the various mean free paths and albedo reads,  $1/l = nt\bar{t}/4\pi = an\Im t/k = a/l_{ex}$ .

## Appendix B. Integrals

The following pair of integrals, related to the diagrams in figure 1, appear throughout the work:

$$\begin{aligned} I_1(\mathbf{q}_1) &= \int \frac{d^3p}{(2\pi)^3} G_0(\mathbf{p} + \mathbf{q}_1)\bar{G}_0(\mathbf{p}) \\ I_2(\mathbf{q}_1, \mathbf{q}_2) &= \int \frac{d^3p}{(2\pi)^3} G_0(\mathbf{p} + \mathbf{q}_1)G_0(\mathbf{p} - \mathbf{q}_2)\bar{G}_0(\mathbf{p}) \end{aligned} \tag{B.1}$$

A mesoscopic approximation to these functions is sufficient for our purposes.

The first integral  $I_1$  is the ladder kernel of the SM equation and may be obtained most conveniently from the mesoscopic real space form as the Fourier transform of  $\mathcal{M}_0 = e^{-r/l}/4\pi lr^2$ ,

$$\tilde{\mathcal{M}}_0(q) = \frac{1}{ql} \int_0^\infty dr \frac{\sin qr}{r} e^{-r/l} = \frac{\tan^{-1}(ql)}{ql} = A_1(ql) \tag{B.2}$$

Hence the free green function of the SM equation is  $\mathcal{G}_0(q) = 1/(1 - A_1(ql))$ .

The integrals (B.1) can also be evaluated directly by performing the integrals over the magnitude of the loop momenta, and then expanding the angular integrals in  $1/kl$  to find the following mesoscopic limits:

$$\begin{aligned} I_1(\mathbf{q}_1) &\rightarrow \frac{l}{4\pi} A_1(q_1 l) \\ I_2(\mathbf{q}_1, \mathbf{q}_2) &\rightarrow \frac{il^2}{8\pi k} A_2(\mathbf{q}_1, \mathbf{q}_2) \end{aligned} \quad (\text{B.3})$$

The properties of the angular integrals  $A_1, A_2$  are discussed in appendix C.

### Appendix C. Angular Integrals

The definition and properties of the angular integrals  $A_1, A_2$  are given in this appendix.

$$A_1(q) = \frac{1}{4\pi} \int_{S_2} d\hat{p} \frac{1}{1 + i\mathbf{q}\cdot\hat{\mathbf{p}}} = \frac{\tan^{-1}(q)}{q} \quad (\text{C.1})$$

The integral  $A_1$  is real and depends only on the length of the vector  $\mathbf{q}$ . Note that  $A_1(0) = 1$ , and that the expansion for small  $q$  is  $A_1(q) = 1 - q^2/3 + q^4/5 + O(q^6)$ . At large  $q$ ,  $A_1$  behaves as  $\pi/2q$ .

We also require a slightly more complicated integral,

$$A_2(\mathbf{q}_1, \mathbf{q}_2) = \frac{1}{4\pi} \int_{S_2} d\hat{p} \frac{1}{1 + i\mathbf{q}_1\cdot\hat{\mathbf{p}}} \frac{1}{1 - i\mathbf{q}_2\cdot\hat{\mathbf{p}}} \quad (\text{C.2})$$

This expression is again real due to the symmetry  $\hat{\mathbf{p}} \rightarrow -\hat{\mathbf{p}}$ . It obeys the following,

$$A_2(\mathbf{q}, \mathbf{0}) = A_2(\mathbf{0}, \mathbf{q}) = A_1(q) \quad (\text{C.3})$$

Although a simple expression for this integral is not available, for the purposes here it is sufficient to consider an expansion in the incoming momentum. To leading order in small  $q_1$  we have,

$$A_2(\mathbf{q}_1, \mathbf{q}_2) \approx A_1(q_2) - \frac{\mathbf{q}_1\cdot\mathbf{q}_2}{q_2^2} (1 - A_1(q_2)) = A_1(q_2) - \mathbf{q}_1\cdot\mathbf{q}_2 A_3(q_2) \quad (\text{C.4})$$

where we have introduced  $A_3(q) = (1 - A_1(q))/q^2$ . If both  $q_1$  and  $q_2$  are small,  $A_2(\mathbf{q}_1, \mathbf{q}_2) \approx 1 - \mathbf{q}_1\cdot\mathbf{q}_2/3$ . Some further properties involving angular integrals of  $A_2$  are also needed,

$$\begin{aligned} \frac{1}{4\pi} \int_{S_2} d\hat{q} A_2(\mathbf{q}, \mathbf{q}_2) &= A_1(q) A_1(q_2) \\ \frac{1}{4\pi} \int_{S_2} d\hat{q} \mathbf{q}_1\cdot\mathbf{q} A_2(\mathbf{q}, \mathbf{q}_2) &= \mathbf{q}_1\cdot\mathbf{q}_2 q^2 A_3(q) A_3(q_2) \end{aligned} \quad (\text{C.5})$$

## Appendix D. Matrix Formalism

Consider each of the 3 diagrams in figure 1 as a separate entry in a  $3 \times 3$  matrix. The matrix version of the vertex for small incoming momentum (3.7) is

$$\begin{aligned}
 V_1 &= -\frac{4\pi l^2}{3} \mathbf{Q}_1 A_1(p'l) + \mathbf{p} \cdot \mathbf{p}' 4\pi l^2 \mathbf{P}_1 A_3(p'l) \\
 \mathbf{Q}_1 &= \frac{-3}{4\pi l} \begin{pmatrix} t\bar{t}/4\pi & & \\ & it/2k & \\ & & -i\bar{t}/2k \end{pmatrix} \\
 \mathbf{P}_1 &= \frac{l}{4\pi} \begin{pmatrix} 0 & & \\ & it/2k & \\ & & -i\bar{t}/2k \end{pmatrix}
 \end{aligned} \tag{D.1}$$

This form is preserved at higher order, though  $\mathbf{Q}$  and  $\mathbf{P}$  are no longer diagonal, and the measured charge/dipole moment is given by the sum of all entries of the respective matrix.

The advantage of the matrix formalism is in connecting vertices using a propagator that can take account of the appropriate combinatorics discussed in the text. To only include ladder diagrams we write,

$$\mathbf{G} = \begin{pmatrix} 1 & 1 & 1 \\ 1 & 1 & 1 \\ 1 & 1 & 1 \end{pmatrix} \mathcal{G}_0 \tag{D.2}$$

To also include crossed diagrams we have,

$$\mathbf{G} = \begin{pmatrix} 2 & 2 & 2 \\ 2 & 2 & 1 \\ 2 & 1 & 2 \end{pmatrix} \mathcal{G}_0 \tag{D.3}$$

The higher order diagrams are summed to give,

$$\begin{aligned}
 \mathbf{Q} &= \mathbf{Q}_1 \left( 1 + \frac{4\pi}{3l} \mathbf{G} \mathbf{Q}_1 \right)^{-1} \\
 \mathbf{P} &= \mathbf{P}_1 \left( 1 - \frac{4\pi}{3l^3} \mathbf{G} \mathbf{P}_1 \right)^{-1}
 \end{aligned} \tag{D.4}$$

When evaluated using the ladder propagator we recover the result (3.12). When the crossed diagrams are included we must explicitly drop terms that are subleading in the mesoscopic approximation and are left with the result,

$$Q = \frac{Q_1}{1 + \frac{2\sigma_{el}}{l}(1/a_e - 1)B_1} + Q_1 \frac{\sigma_{el}}{l}(1/a_e - 1)B_1 = \frac{Q_1}{1 + \frac{8\pi}{3}Q_1 B_1} + \frac{4\pi}{3}Q_1^2 B_1 \tag{D.5}$$

$$P = \frac{P_1}{1 + 6\sigma_{el}l(1/a_e)B_2} + P_1 3\sigma_{el}l(1/a_e)B_2 = \frac{P_1}{1 + 8\pi P_1 B_2} + 4\pi P_1^2 B_2 \tag{D.6}$$

where the added terms correct for the fact that the two-scatterer diagram has no time-reversed counterpart. The main change is thus a factor of two in the  $B$ 's compared with the ladder result (3.12).

## Appendix E. Classical scattering from a sphere

We collect certain results concerning amplitude scattering from a sphere [7]. A scattering solution for a field obeying the wave equation, with incoming part  $e^{ikz}$ , and symmetric object, is

$$\phi = \sum_l i^l \sqrt{4\pi(2l+1)} \left( j_l(kr) + a_l h_l^{(1)}(kr) \right) Y_{l0}(\theta) \quad (\text{E.1})$$

The coefficients  $a_l$  are determined by the boundary conditions. Besides Dirichlet ( $D$ ) and Neumann ( $N$ ) conditions, a more general possibility is to assume a surface impedance,  $Z$ , and require,  $\partial_t \phi = ik\phi = Z\partial_r \phi$ , on the surface. These coefficients are the same as the ones appearing in the green function (5.1).

By calculating the fluxes we find the following cross sections,

$$\begin{aligned} \sigma_{el} &= \frac{4\pi}{k^2} \sum_l (2l+1) |a_l|^2 \\ \sigma_{abs} &= \frac{-4\pi}{k^2} \sum_l (2l+1) \left( |a_l|^2 + \frac{a_l + \bar{a}_l}{2} \right) \\ \sigma_{tot} &= \sigma_{el} + \sigma_{abs} \end{aligned} \quad (\text{E.2})$$

For  $D$  and  $N$  conditions,  $\sigma_{abs} = 0$ , and for a large sphere ( $kR \gg 1$ ),  $\sigma_{tot} = 2\pi R^2$ .

## Appendix F. Integrals for Spherical Object

In the text we have only discussed the position space form of the bare vertex for the spherical object. The following representation in momentum space is convenient for calculations,

$$\begin{aligned} \tilde{V}_1(\mathbf{p}, \mathbf{p}') &= \int d^3r \int d^3r' e^{-i\mathbf{p}\cdot\mathbf{r}} e^{i\mathbf{p}'\cdot\mathbf{r}'} V_1(\mathbf{r}, \mathbf{r}') \\ &= \frac{4\pi}{l_{ex}} \int_R dr r^2 \int_R dr' r'^2 \sum_{ll'} (\bar{a}_{l'} g_l^{(0)} \bar{g}_{l'}^{(1)} + a_l \bar{g}_{l'}^{(0)} g_l^{(1)} + a_l \bar{a}_{l'} g_l^{(1)} \bar{g}_{l'}^{(1)}) \\ &\quad \times \int d\hat{r} \int d\hat{r}' e^{-i\mathbf{p}\cdot\hat{r}} e^{i\mathbf{p}'\cdot\hat{r}'} \frac{(2l+1)}{4\pi} \frac{(2l'+1)}{4\pi} P_l(\cos\gamma) P_{l'}(\cos\gamma) \end{aligned} \quad (\text{F.1})$$

Where  $\gamma$  is the angle between the two vectors  $\hat{r}$  and  $\hat{r}'$ . We have written the mean free path as  $l_{ex}$  in this formula to prevent confusion with the angular momentum quantum number.

Although not tractable, this form can be used to prove the following two formulae which are the analogs of the integration formulae (C.5) in appendix C.

$$\begin{aligned}
& \int d^3r \int d^3r' a(r)b(r') e^{i\mathbf{p}' \cdot \mathbf{r}'} V_1(\mathbf{r}, \mathbf{r}') \\
&= \frac{4\pi l}{3} Q_1 \int_R dr a(r) e^{(R-r)/l} \int_R dr' \frac{\sin p' r'}{p' r'} b(r') e^{(R-r')/l} \\
& \int d^3r \int d^3r' a(r)b(r') i(\mathbf{p} \cdot \mathbf{r}) e^{i\mathbf{p}' \cdot \mathbf{r}'} V_1(\mathbf{r}, \mathbf{r}') \\
&= -\mathbf{p} \cdot \mathbf{p}' \frac{4\pi l^3}{(R+l)^2} P_1 \int_R dr r a(r) e^{(R-r)/l} \int_R dr' \left( \frac{\sin p' r'}{p'^3 r'^2} - \frac{\cos p' r'}{p'^2 r'} \right) b(r') e^{(R-r')/l}
\end{aligned} \tag{F.2}$$

Where  $a(r)$  and  $b(r)$  are smooth functions. The asymptotic form of the Bessel functions has been used and oscillating terms which contribute at higher order in  $1/kl$  have been dropped in accordance with the mesoscopic approximation.

The functions  $A_1^{(R)}$  and  $A_3^{(R)}$  are defined as follows,

$$\begin{aligned}
A_1^{(R)}(ql, R/l) &= \int_R^\infty \frac{dr}{l} \frac{\sin qr}{qr} e^{(R-r)/l} = \frac{1}{4\pi} \int_{S_2} d\hat{\mathbf{p}} \frac{e^{-i\mathbf{q} \cdot \hat{\mathbf{p}} R}}{1 + i\mathbf{q} \cdot \hat{\mathbf{p}} l} \\
A_3^{(R)}(ql, R/l) &= \frac{1}{q(R+l)} \int_R^\infty \frac{dr}{l} \left( \frac{\sin qr}{q^2 r^2} - \frac{\cos qr}{qr} \right) e^{(R-r)/l}
\end{aligned} \tag{F.3}$$

They have the following limits as  $R \ll l$ ,

$$\begin{aligned}
A_1^{(R)}(ql, R/l) &\rightarrow A_1(ql) \\
A_3^{(R)}(ql, R/l) &\rightarrow A_3(ql) = \frac{(1 - A_1(ql))}{(ql)^2}
\end{aligned} \tag{F.4}$$

## References

- [1] P.N. den Outer, Th.M. Nieuwenhuizen and Ad Lagendijk, *J.Opt.Soc.Am.A* **10**, 1209 (1993).
- [2] H.M.J. Boots, J.H.M. Neijzen, F.A.M.A. Paulissen M.B. van der Mark and H.J. Cornelissen, *Liquid Crystals* **22**, 255-264 (1997).
- [3] S. Chandrasekar, *Radiative Transfer*, (Dover, New York, 1960).
- [4] Th.M. Nieuwenhuizen, Lecture notes (in Dutch) (University of Amsterdam, 1993) ; M.C.W. van Rossum and Th.M. Nieuwenhuizen, submitted to *Rev. Mod. Phys.*
- [5] J.M. Luck and Th.M. Nieuwenhuizen, to appear.
- [6] Th.M. Nieuwenhuizen, A. Lagendijk, and B.A. van Tiggelen, *Physics Lett. A* **169** (1992) 191.
- [7] J.D. Jackson, *Classical Electrodynamics*, Wiley, New York (1975) ; J.J. Bowman, T.B.A. Senior and P.L.E. Uslenghi (eds), *Electromagnetic and Acoustic Scattering by Simple Shapes*, North Holland, Amsterdam (1969).
- [8] J.C.J. Paasschens and G.W. 't Hooft, *J. Opt. Soc. A.*, submitted; J.C.J. Paasschens, PhD thesis (Leiden, 1997).